crystals

MDPI

Article

Investigation on the Cu-Dopant-Induced Modulation Effect on the Optoelectronic Efficiency and the Stability of $CsPbBr_3$ Perovskites

Yinuo Ma [1], Fangchao Liu [1], Hao Jiang [1], Jialin Wu [1], Qiuhong Huo [1], Zhongchen Wu [1,2], Wei-Yan Cong [1,*] and Ying-Bo Lu [1,*]

[1] School of Space Science and Physics, Shandong University, Weihai 264209, China; mayinuo@mail.sdu.edu.cn (Y.M.); you_mu_sdu@163.com (F.L.); 202000830016@mail.sdu.edu.cn (H.J.); jialin_wu@mail.sdu.edu.cn (J.W.); huoqh@sdu.edu.cn (Q.H.); z.c.wu@sdu.edu.cn (Z.W.)

[2] Shandong Key Laboratory of Optical Astronomy and Solar-Terrestrial Environment, Institute of Space Sciences, Shandong University, Weihai 264209, China

* Correspondence: cong_wy@sdu.edu.cn (W.-Y.C.); lyb@sdu.edu.cn (Y.-B.L.); Tel.: +86-131-8110-4093 (W.-Y.C.); +86-138-6316-0610 (Y.-B.L.)

Abstract: This study explores the use of Cu dopant to improve the optoelectronic properties and stability of $CsPbX_3$ perovskites for blue-light-emitting diode material. The addition of Cu causes the metal octahedron of orthorhombic $CsPbBr_3$ to shrink, which relaxes the lattice strain from the distortion and twisting of the $[PbX_6]$ octahedron and reduces energy from Jahn–Teller effects. A crystal orbital Hamilton population (COHP) analysis reveals that the Cu-Br bond in the $[CuX_6]$ octahedron has a higher integrated projected COHP (IpCOHP), and the strong hybridization between the Cu-3d and Br-4p bond enhances the bond interaction and the whole crystalline lattice. The addition of Cu dopants in $CsPbBr_3$ perovskites results in a stronger framework that suppresses intrinsic defects like Br vacancies, leading to enhanced photoluminescence (PL) performance. Additionally, the Cu-3d orbitals contribute to the valence band and increase the band gap, resulting in a blue shift of the luminescence from Cu-doped $CsPbBr_3$. These findings indicate that Cu dopants significantly improve the luminescence efficiency and the stability of $CsPbBr_3$ perovskites, making them suitable for blue light LED applications.

Keywords: $CsPbBr_3$ perovskites; Cu dopant; crystal orbital Hamilton population; blue luminescence; stability

check for updates

Citation: Ma, Y.; Liu, F.; Jiang, H.; Wu, J.; Huo, Q.; Wu, Z.; Cong, W.-Y.; Lu, Y.-B. Investigation on the Cu-Dopant-Induced Modulation Effect on the Optoelectronic Efficiency and the Stability of $CsPbBr_3$ Perovskites. *Crystals* **2023**, *13*, 1180. https://doi.org/10.3390/cryst13081180

Academic Editor: Raphaël P. Hermann

Received: 24 June 2023
Revised: 11 July 2023
Accepted: 22 July 2023
Published: 28 July 2023

Copyright: © 2023 by the authors. Licensee MDPI, Basel, Switzerland. This article is an open access article distributed under the terms and conditions of the Creative Commons Attribution (CC BY) license (https://creativecommons.org/licenses/by/4.0/).

1. Introduction

In recent years, halide perovskites, including $MAPbI_3$ and $MAPbBr_3$, have emerged as strong contenders for high-performance solar cells. Nawishta et al. have successfully grown single-layer and multilayer $MAPbIBr_2$ thin films, which show sharper absorption peaks in the visible region, suggesting their potential for application in optoelectronic and photovoltaic devices [1–5]. Among these, all-inorganic perovskites like $CsPbX_3$ have garnered significant attention for their exceptional stability and optoelectronic properties. Lots of studies highlight the potential use of inorganic halide perovskites as luminescent materials. The band gaps of these materials can be adjusted to cover the entire visible region. Additionally, $CsPbX_3$ perovskites exhibit a narrow emission line width of 12–42 nm and a high photoluminescence quantum yield (PLQY) of 50–90%. Notably, $CsPbBr_3$ emits green light [6] and $CsPbI_3$ emits red light [7], both with a luminous quantum yield of over 90%. As is well-known, the blue luminescence is the most important in applications of the LED, but the all-inorganic $CsPbX_3$ perovskites are frustrated in this field [8–14].

Numerous methods have been utilized to enhance the blue luminescence efficiency of $CsPbX_3$ perovskites. One such method involves doping Cl anions in the Br-halide

perovskites, resulting in mixed-anion halide perovskites that emit blue light. This was demonstrated by Loredana et al. in 2015 [15,16]. However, the presence of these mixed anions causes lattice mismatch, which can lead to a deterioration in the crystalline structure and limit the PLQY of the blue luminescence to less than 40%. To address this issue, some reports have explored the size effect of perovskites. For example, Wang et al. fabricated $CsPbBr_3$ perovskite quantum dots that emit light with a shorter wavelength [9]. Despite their potential in optoelectronic applications, perovskites have been limited by their thermal instability. Fortunately, recent research has shown that metallic impurity doping can effectively enhance their optoelectronic properties, including PLQY and thermal stability. For instance, the addition of Sn into $CsPbBr_3$ perovskites has been found to significantly increase the PLQY from 45% to an impressive 83% in $CsPb_{1-x}Sn_xBr_3$ [17,18]. Shen et al. successfully created a stable $CsPb_{0.64}Zn_{0.36}I_3$ crystal with a high PLQY of 98.5% through Zn doping. Furthermore, researchers have made significant advancements in the field of Cu doping in perovskite materials. This is attributed to the similarity in oxidation states between Cu and Pb, with Cu exhibiting a considerably smaller atomic radius than Pb. Additionally, the electronegativity disparity between Cu and Br surpasses that of Pb and Br. As a result, numerous studies have been conducted to explore the effects of Cu doping on the optoelectronic properties of semiconductor materials. The brightness of the light-emitting diodes (LEDs) made from Cu-doped $CsPbI_3$ perovskites is high, measuring at 1270 cd/m^2. Additionally, the red luminescence of this device can remain stable in air for up to 35 days [19]. Yu et al. discovered that the bandgap of $Cs_2AgSbCl_6$ double perovskites can be significantly altered through the use of Cu dopants [20]. Cu doping can alter the electronic interaction within $CsPbBr_3$ perovskites [21], resulting in an increased bandgap that facilitates the blue light emission. Bi et al. have experimentally demonstrated that substituting Cu for Pb in $CsPbX_3$ perovskites enhances the PLQY from 23% to an impressive value of 80%. Furthermore, this high PLQY can be sustained for 30 days under 60% relative humidity [22,23].

The remarkable optoelectronic properties exhibited by Cu-doped $CsPbBr_3$ perovskites have been attributed to the suppression of intrinsic defects. However, the mechanism behind this phenomenon and its impact on the photoluminescence quantum yield and stability require further exploration. Previous studies have also indicated that $CsPbBr_3$ may undergo a phase transition from orthorhombic to cubic when exposed to visible light or fabricated in nano scales [24]. This paper aims to investigate the impact of Cu dopant on the $CsPbBr_3$ perovskite lattice and determine if different phases alter its influence. Through an analysis of defect formation energies, geometric distortions, bonding interactions, and electronic structures, we have found that Cu dopant strengthens the bonding interactions between cation and anion ions in the $CsPbBr_3$ crystal, reducing native defects and increasing co-ordinated numbers of the metallic octahedral. This is helpful in promoting the PLQY and the stability of the lattice as a whole. Our research offers a more extensive theoretical foundation for achieving high-quality all-inorganic $CsPbX_3$ perovskites that emit blue light.

2. Calculation Methods

The theoretical simulations and analyses in this paper are performed via density functional theory, which is implemented in the Vienna ab initio simulation package (VASP) [25,26]. We use the generalized gradient approximation (GGA) function and Perdew–Burke–Ernzerhof (PBE) model to deal with the exchange and correlation of electrons [27]. Meanwhile, we use the Heyd–Scuseria–Ernzerh of hybridized function (HSE06) with the shielding parameter 0.25 to obtain a more accurate bandgap [28]. The projector-enhanced wave (PAW) method is used to deal with the interaction between electrons and ions [29]. The cutoff energy, the convergence accuracy, and the residual force are set to 400 eV, 1×10^{-4} eV per atom, and 0.01 eV, respectively. In addition, we use a $2 \times 4 \times 4$ Monkhorst–Pack mesh to integrate in Brillouin zone. The crystal orbital Hamilton population (COHP) [30,31] calculations are carried out by LOBSTER program, in which

the chemical bonds involved are: (1) 4s, 4p, and 3d for Cu; (2) 4s and 4p for Br; and (3) 6s, 6p, and 5d for Pb, respectively.

3. Results and Discussion

3.1. Geometric Properties

The physical properties of solid materials are determined by their geometric structures, which can be affected by intrinsic defects or external dopants. Understanding the optoelectronic properties of $CsPbBr_3$ perovskites requires a thorough examination of these geometric variations. At room temperature, $CsPbBr_3$ crystallizes in the orthorhombic phase with the space group Pnma, as depicted in Figure 1. The perovskites consist of [$PbBr_6$] metal octahedra, with Cs ions occupying the vacancies between these octahedra due to their larger radii. The relaxed lattice parameters of the $CsPbBr_3$ supercell are 16.53 Å, 8.50 Å, and 11.92 Å, respectively. Perovskites are commonly synthesized with intrinsic defects, which can reduce the PLQY by acting as non-radiative recombination centers. However, these defects also play a major role in the decomposition of perovskite materials when exposed to air, due to their strong affinity for water and oxygen molecules. This can lead to a decrease in stability for perovskite materials [32]. The paper focuses on investigating the intrinsic defects in $CsPbBr_3$, namely, Cs vacancy (V_{Cs}), Pb vacancy (V_{Pb}), and Br vacancy (V_{Br}). The configuration of the $CsPbBr_3$ supercell with V_{Br} is depicted in Figure 1c. The formation energy is used to determine the likelihood of defect formation, which is calculated using Equation (1).

$$E_f = E_{df} - E_{ini} + \sum_i n_i\mu_i - \sum_j n_j\mu_j \quad (1)$$

where E_{ini} represents the total energy of the defect-free supercell, E_{df} represents the total energy of the defect-containing system. μ_i and μ_j are the chemical potentials of the elements involved in the formation of defects, in which the chemical potentials of the metal cations are obtained from the bulk materials, while the chemical potential of the Br atom is obtained from the gaseous material. For example, if we calculate the defect formation energy of $CsPbBr_3$ with a defect complex composited by the Cu-substitutional Pb (Cu_{Pb}) and a Br vacancy ($Cu_{Pb}V_{Br}$), then $E_f = E_{df} - E_{ini} + \mu_{Br} + \mu_{Pb} - \mu_{Cu}$. The calculated defect formation energies of various defects are listed in Table 1.

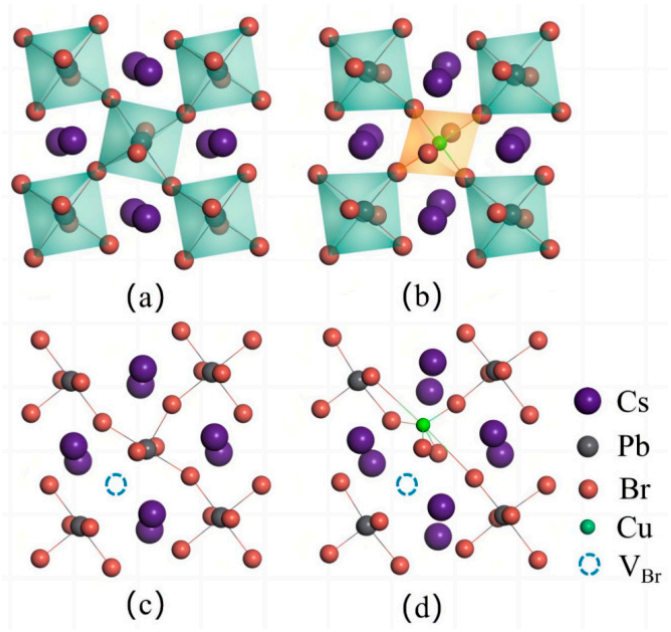


Figure 1. Geometric structures of (**a**) $CsPbBr_3$ supercell, (**b**) $CsPb_{0.875}Cu_{0.125}Br_3$ supercell, (**c**) V_{Br}-containing $CsPbBr_3$ supercell, and (**d**) $Cu_{Pb}V_{Br}$ complex containing $CsPb_{0.875}Cu_{0.125}Br_3$ supercell, respectively.

Table 1. Formation energies (E_f) of various defects in $CsPbBr_3$ and $CsPb_{0.875}Cu_{0.125}Br_3$ systems.

Defects	V_{Cs}	V_{Pb}	V_{Br}	$Cu_{Pb}V_{Cs}$	$Cu_{Pb}V_{Pb}$	$Cu_{Pb}V_{Br}$
E_f (eV)	4.26	3.74	2.90	6.69	5.69	2.92

One of the intrinsic defects in $CsPbBr_3$ materials is the V_{Br}, which has the lowest formation energy among the defects. On the other hand, the value of V_{Cs} is the highest among the defects. This means that, in the $CsPbBr_3$ supercell, V_{Cs} is the most difficult defect to form, while V_{Br} is the easiest defect to form. Then, V_{Br} vacancies are believed to be responsible for the deterioration of the PLQY in the pristine $CsPbBr_3$ perovskites. These results are consistent with previous reports [15]. Therefore, these vacancies should be suppressed to regulate the stability and the optoelectronic properties of perovskites [33]. Previous reports have suggested that the Cu substitutional defect strongly affects the geometric structure of $CsPbBr_3$ perovskites. To investigate this effect, we constructed a $CsPb_{0.875}Cu_{0.125}Br_3$ system by replacing a Pb atom with a Cu dopant in the original $CsPbBr_3$ supercell. The introduction of the Cu dopant resulted in a reduction of the lattice parameters of $CsPbBr_3$ to a = 16.35 Å, b = 8.41 Å, and c = 11.79 Å, due to the smaller radius of the Cu ion. According to the X-ray diffraction (XRD) pattern analysis in Figure 2 provided by Bi et al. [23], it is evident that the diffraction peaks shift towards higher angles (increased 2θ values), and the positions of peaks at larger 2θ values also increase. This observation suggests a decrease in the interplanar spacing of the crystal, providing experimental confirmation of the conclusion that the lattice constant is reduced. Interestingly, the Cu dopant can also alter the distribution of intrinsic defects. As shown in Table 1, the formation energies of intrinsic vacancies in $CsPbBr_3$ increases obviously after Cu doping, indicating that the formation of intrinsic defects becomes more difficult after Cu doping, compared with the undoped system. From an alternative standpoint, the reduction in the diameter of the dopant ions leads to the relaxation of lattice stress caused by distortion and compression between adjacent lattices. As a result, this relaxation of lattice stress may also reduce the dislocation density within the crystal, ultimately promoting greater stability of the $CsPbBr_3$ perovskite structure.

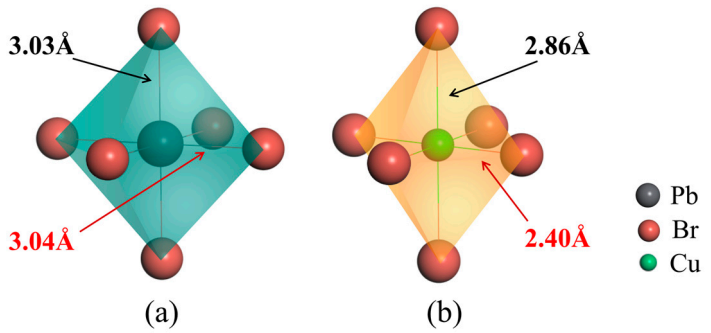


Figure 2. Localized structures of (**a**) $[PbX_6]$ in the pristine $CsPbBr_3$ and (**b**) $[CuX_6]$ in $CsPb_{0.875}Cu_{0.125}Br_3$ supercells, respectively.

To gain a better understanding of the effect induced by Cu dopant on $CsPbBr_3$ perovskites, we focus on studying the geometric changes caused by the dopant. According to the commonly held view, the stability of a perovskite can be evaluated based on the tolerance factor t, which is defined in Equation (2).

$$t = \frac{R_A + R_X}{\sqrt{2}(R_B + R_X)} \quad (2)$$

Among them, R_A, R_B, and R_X are the radii of composition ions in ABX_3 perovskites. The radii used in this work are shown in Table 2.

Table 2. Crystal radii (CR) [34] and the co-ordination numbers (CN) of ions in $CsPbBr_3$ systems.

Ion	Cu^{2+}	Cs^{1+}	Br^{1-}	Pb^{2+}
CN	6	12	6	6
CR(pm)	87	202	182	133

According to theoretical analysis, perovskites can exist steadily within the range of 0.77–1.10 for the value of *t*. As *t* approaches 1, the stability of the perovskite structure is enhanced. From Table 2 and Formula (2), it can be observed that the tolerance factor of $CsPbBr_3$ is 0.86, which deviates from the ideal value of 1. This deviation is one of the reasons why $CsPbBr_3$ tends to crystallize in the orthorhombic phase under normal conditions, resulting in a distorted perovskite structure. By calculating *t* using the radius of the Cu^{2+} ion instead of the original Pb^{2+} ion, we arrive at a value of 1.01, which is almost ideal for perovskites. This indicates that the metal–halogen octahedra frameworks in the $CsPbBr_3$ lattice are strengthened after Cu doping. The more stable perovskite structure confirms our earlier findings on the formation energies, which suggest that the $CsPbBr_3$ lattice is less prone to intrinsic defects due to its increased resistance to destruction.

To gain a better understanding of the results, we conducted extensive simulations on the localized structures and bonding interactions for the $CsPbBr_3$ lattice before and after Cu doping. The results from Figure 2 indicate that the Pb-Br bond lengths in the $[PbBr_6]$ metal octahedron of the original $CsPbBr_3$ lattice are approximately 3.03 Å prior to Cu doping. Upon substitution of Pb with Cu dopant, the 3.03 Å Cu-Br bond lengths in the $[CuX_6]$ octahedron reduce to 2.86 Å, while the 3.04 Å Cu-Br bond lengths decrease to 2.40 Å, resulting in the shrinkage of the octahedron and the elongating of the octahedron. In accordance with rigorous academic conventions, it is imperative to consider not only the beneficial impacts arising from doping-induced distortions but also their potential drawbacks. When examining the reduction in Cu-Br bond length, it becomes evident that the bromine atom involved in forming the Cu-Br bond experiences elongation due to its proximity to the surrounding lead bromide octahedra. However, it is important to note that the degree of deformation along this axis is not particularly substantial, and it is limited to the nearest neighboring Pb-Br octahedra, thereby restricting its impact on the formation energy of bromine vacancy defects.

The compact lattice resulting from the contraction of the bond length of the $[CuX_6]$ octahedron makes it difficult to lose compositional atoms, thus increasing the formation energy of the V_{Br} defect. Additionally, the distortion of the metal octahedron due to the Jahn–Teller effect results in an energy gain and reduces the energy of the entire lattice system, which will be further discussed in subsequent sections. Furthermore, the shrinkage of the metal octahedral cage reduces the lattice strain caused by the rotation and twisting of the $[PbBr_6]$ octahedron in the pristine $CsPbBr_3$ lattice. The stability of $CsPbBr_3$ perovskites is enhanced by three factors. Additionally, we observed that lattice distortion only occurs in the $[PbX_6]$ metal octahedra closing to the $[CuX_6]$ octahedron, while the Pb-Br bonds further away from the $[CuX_6]$ octahedron remain relatively unchanged. This indicates that Cu dopant only induces a short-range interaction in $CsPbBr_3$.

3.2. Electronic Properties

The crystal orbital Hamilton population (COHP) analyses provide a direct measure of the bonding strength in $CsPbBr_3$ systems. As presented in Table 3, the integrated projected COHP (IpCOHP) for the Pb-Br bonds are 1.63 eV before Cu doping and 1.80 eV after Cu doping, respectively. This indicates that Cu doping strengthens the bond in the nearest neighboring $[PbBr_6]$ octahedron. The Cu-Br bond within the $[CuBr_6]$ octahedron has a significantly higher IpCOHP value of 5.04 eV. This finding agrees with our aforementioned conclusions, which indicate that the reduction of the metal-Br bonds and the shrinkage of the metal octahedra contribute to the strengthening of the lattice. This statement suggests that, by preventing the breaking of bonds, the formation of intrinsic defects can be

suppressed. According to Figure 3, the bonding energy peak of the Cu-Br bond is approximately −13 eV, which is significantly lower than that of the Pb-Br bond. This reduction in energy of the system contributes to the stability of the crystal. The study shows that the Pb-Br bond is primarily formed by the interaction of Pb-6p and Br-4p orbitals, while the Cu-Br bond is formed by the interaction of Cu-3d and Br-4p orbitals. The bonding energy between Cu-3d and Br-4p is lower than that between Pb-6p and Br-4p orbitals, but the bonding strength of the former is much higher than the latter. This suggests that the strong hybridization resulting from Cu-3d orbitals enhances the bonding interaction between Cu-3d/Br-4p bonds, thereby reducing the total energy of the supercell system.

Table 3. The lengths (Å) and the IpCOHP (eV per cell) for the metal-Br bonds in $CsPbBr_3$ and $CsPb_{0.875}Cu_{0.125}Br_3$ systems, respectively.

System	Bond	Bond Length	−IpCOHP
$CsPbBr_3$	Pb-Br	3.03	1.63
$CsPb_{0.875}Cu_{0.125}Br_3$	Cu-Br	2.40	5.04
$CsPb_{0.875}Cu_{0.125}Br_3$	Pb-Br	2.97	1.80

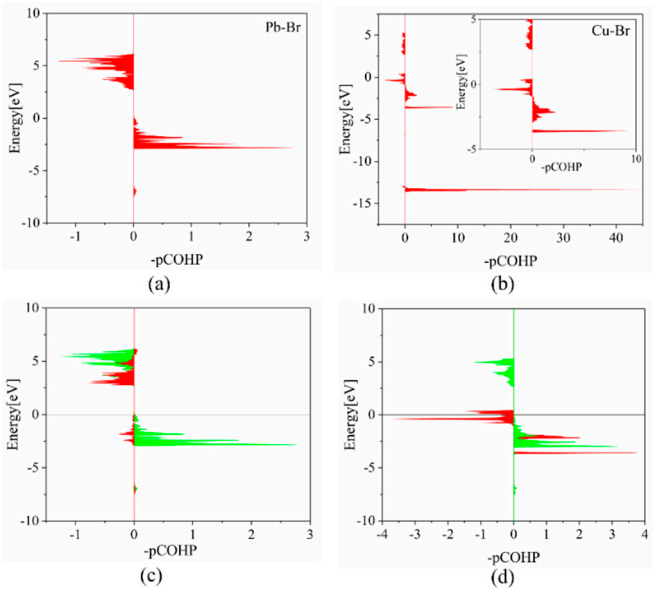


Figure 3. COHP analyses for (**a**) Pb–Br bond in pristine $CsPbBr_3$ and (**b**) Cu–Br bond in $CsPb_{0.875}Cu_{0.125}Br_3$, respectively. Orbital COHP analyses for (**c**) Pb [6p]-Br [4s] (red) and Pb [6p]-Br [4p] (green) in pristine $CsPbBr_3$ and (**d**) Cu [3d]-Br [4p] (red) and Pb [6p]-Br [4p] (green) in $CsPb_{0.875}Cu_{0.125}Br_3$ supercell, respectively. The inset in (**b**) represents the enlarged COHP analyses with the energy from −5 eV to 5 eV for Cu–Br bond in $CsPb_{0.875}Cu_{0.125}Br_3$.

Our analysis of the bonding interactions and geometric structures is in agreement with the findings on formation energies. Specifically, the introduction of Cu doping results in a more compact $CsPbBr_3$ lattice with strengthened bonds, reducing the likelihood of intrinsic defects forming. This increases in the co-ordination number of cations and improved lattice order, which aligns with previous experimental observations [23].

To investigate the effect of copper doping on the optoelectronic properties of the $CsPbBr_3$ system, we also calculated the band structure and the density of states (DOS) using the hybrid density functional (HSE) method to obtain more precise results. As shown in Figure 4a,b, the undoped $CsPbBr_3$ system has a bandgap of 2.38 eV. After copper doping, the band gap increases to 2.91 eV. This blue shift of the bandgap is consistent with experimental observations and meets the original goal of extending the luminescence of $CsPbBr_3$ to blue light. The blue shift can provide an effective idea for us to find complementary blue-emitting LED materials. From the plotted density of states (PDOS) plots in Figure 4c,d,

it can be seen that the contribution of Cs ions to the band edge is negligible, which has little effect on the electron transport. In the undoped $CsPbBr_3$ system, the valence band maximum (VBM) is mainly dominated by Br-4p orbitals, while the conduction band minimum (CBM) is mainly contributed by Pb-6p orbitals. After doping copper, the VBM of the $CsPb_{0.875}Cu_{0.125}Br_3$ system is strongly influenced by the Cu-3d orbital—i.e., Cu-3d is strongly hybridized with Br-4p—while the CBM continues to be controlled by the Pb-6p orbital, leading to the increase of the bandgap accordingly. That is to say, the Cu-3d orbital mainly changes the energy band structure and enlarges the band gap, which is consistent with the COHP analysis we mentioned earlier.

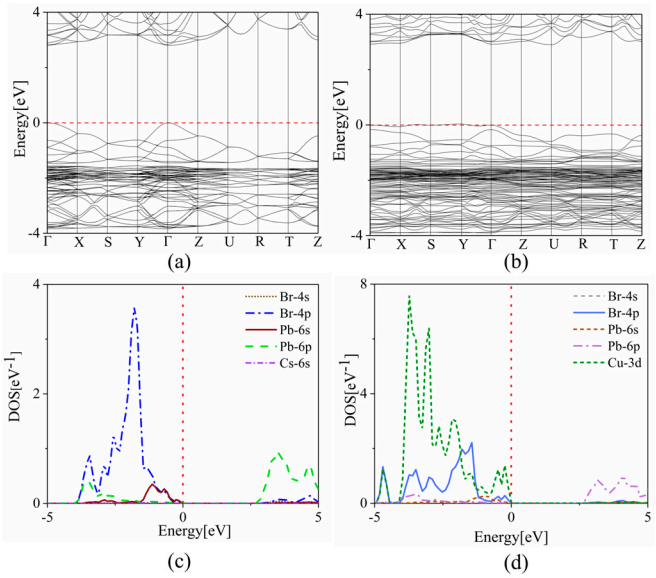


Figure 4. The band structures of (**a**) $CsPbBr_3$ and (**b**) $CsPb_{0.875}Cu_{0.125}Br_3$ systems, respectively. The partial density of states of (**c**) $CsPbBr_3$ and (**d**) $CsPb_{0.875}Cu_{0.125}Br_3$ systems, respectively. The red dash line represents the Fermi level and the black line represents the relationship between the energy of the electron and its momentum.

In order to understand the interaction of Cu-3d orbitals in the $CsPb_{0.875}Cu_{0.125}Br_3$ lattice, we take the orbital angular momentum I into account. The 3d orbit of Cu is composed of d_{xy}, d_{xz}, d_{yz}, $d_{x^2-y^2}$, and d_{z^2}. Ideally, these five orbitals are degenerate. But, as discussed above, when Cu substitutes the Pb position to form the Cu_{Pb} defect in $CsPbBr_3$ perovskites, the $[CuX_6]$ octahedron shrinks and changes into an elongated octahedron, and the five-fold degenerate 3d orbit of Cu then splits into the e_g doublet states and t_{2g} triplet states. This lowers the total energy of $CsPbBr_3$ systems and is beneficial to their stability.

The analysis in Figure S3 (see Supplementary Materials) shows that the refractive index of the perovskite material increases after doping with Cu. This indicates that the interaction of the material with light is enhanced, resulting in a decrease in the propagation velocity of light within the doped perovskite material. As a result, the material may become more opaque, particularly for certain wavelengths of light. This reduction in transparency can impact the propagation and utilization of light within the material. In addition, the increase in refractive index enhances the scattering of astigmatism, leading to a decrease in the optical uniformity of the material. This results in a more complex path of light propagation within the material, which ultimately affects its optical properties. The deterioration of these properties may have a negative impact on the optoelectronic conversion efficiency, causing an increase in light loss and a reduction in photoelectric efficiency. However, it is important to note that the range of change in the refractive index is relatively small, thus limiting its impact on optical performance. Through the calculation of defect propagation energy after doping, we have observed a significant reduction in defects. This indicates

that doping Cu remains a crucial factor for enhancing photoelectric performance, resulting in effective and remarkable improvement.

As previously reported, $CsPbBr_3$ can exist in the cubic phase under certain conditions. Therefore, it is important to consider whether Cu doping could affect the optoelectronic properties of cubic $CsPbBr_3$. In this study, we thoroughly investigate the effects of Cu doping on the geometric structure and, thus, the stability of $CsPbBr_3$ systems, including the distribution of intrinsic defects and bonding interactions. The undoped and Cu-doped $CsPbBr_3$ supercells in the cubic phase are shown in Figure 5; we can see that, after doping, the metal octahedron and the whole lattice also shrink, and the bonding interactions are strengthened, which are illustrated in Figure S1 in the Supplementary Materials. This means that, after Cu doping, the original lattice becomes stronger than before and the intrinsic vacancies are suppressed, acquiring a more stable perovskite structure and the enhancement of PLQY. These findings are similar to that in the orthorhombic phase $CsPbBr_3$. However, as shown in Figure S2 in the Supplementary Materials, the cubic phase $CsPbBr_3$ exhibits an indirect band structure after Cu doping, and the band gap decreases from 2.41 eV to 2.37 eV, which is unfavorable for blue light emitting.

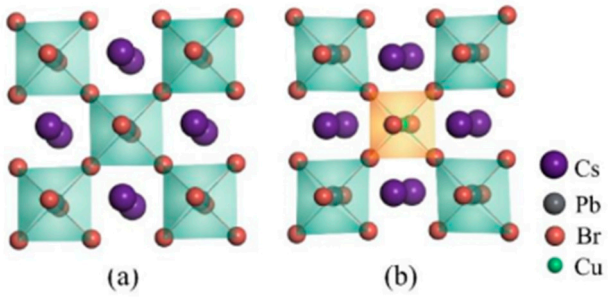


Figure 5. Geometric structures of (**a**) undoped $CsPbBr_3$ supercell and (**b**) $CsPb_{0.875}Cu_{0.125}Br_3$ supercell in cubic phases, respectively.

4. Conclusions

In this study, we conducted a series of theoretical simulations and find that the introduction of Cu dopants results in a contraction of the metal octahedron and the formation of a more compact lattice in the orthorhombic $CsPbBr_3$ materials. Meanwhile, the shrinkage of the metal octahedron relaxes the lattice strain originating from the rotation and the twisting of the $[PbBr_6]$ octahedron in the pristine orthorhombic $CsPbBr_3$ lattice. Owing to the Jahn–Teller effect, the $[CuX_6]$ octahedron distorts to an elongated octahedron to reduce the energy of whole lattice systems. All these factors turn $CsPbBr_3$ perovskites into a more stable state, indicating that the frameworks of this Cu-doped $CsPbBr_3$ become more difficult to break, thus suppressing the intrinsic defect, e.g., Br vacancy. This is believed to be the main contribution to promoting photoluminescence performances. The stronger lattice of Cu-doped $CsPbBr_3$ materials is further confirmed via the COHP analyses, from which we find that the Cu-Br bond in the $[CuX_6]$ octahedron possesses a much higher IpCOHP with the value of 5.04 eV, and the IpCOHP of Pb-Br bond increases from the initial 1.63 eV to 1.80 eV as well. As illustrated in the COHP diagram, the strong hybridization between Cu-3d/Br-4p bonds enhances the bonding interaction and reduces the total energy of the $CsPbBr_3$ system. In addition, after Cu doping, the band gap of $CsPbBr_3$ increases from 2.38 eV to 2.91 eV, resulting from the manifest contribution of Cu-3d orbitals to the valence band. This makes the luminescence of the $CsPbBr_3$ blue shift, benefiting the blue light emitting of perovskites. Finally, through systematic first-principles calculations, we investigated the influence of Cu doping on the geometric structure, electronic properties, and the bonding interactions of the perovskite crystal. Subsequently we acquire a deep understanding of how Cu dopants enhance the optoelectronic properties and the stability of $CsPbBr_3$ perovskite, which is not reported previously. Therefore, our investigations can

help us to modify the physical properties of perovskites by Cu dopant or other transition metals, which could put forward their practical applicability.

Supplementary Materials: The following are available online at https://www.mdpi.com/article/10.3390/cryst13081180/s1, Figure S1: COHP analyses for (a) Pb-Br bond in [PbX_6] octahedron of pristine cubic $CsPbBr_3$, (b) Cu-Br bond in [CuX_6] octahedron of cubic $CsPb_{0.875}Cu_{0.125}Br_3$. The inset in (b) represents the COHP analyses with the energy from −5 eV to 5 eV for Cu-Br bond in $CsPb_{0.875}Cu_{0.125}Br_3$. Figure S2. The band structures of cubic (a) $CsPbBr_3$ and (b) $CsPb_{0.875}Cu_{0.125}Br_3$ systems, respectively. The Partial density of states of cubic (c) $CsPbBr_3$ and (d) $CsPb_{0.875}Cu_{0.125}Br_3$ systems, respectively. All results are calculated via HSE functions. Figure S3: The refractive index of (a) $CsPbBr_3$ and (b) $CsPb_{0.875}Cu_{0.125}Br_3$ systems.

Author Contributions: Conceptualization, Y.-B.L.; methodology, Y.M.; software, F.L.; formal analysis, Y.M., J.W., Q.H. and Z.W.; investigation, H.J. and J.W.; writing—original draft preparation, Y.M.; writing—review and editing, Y.-B.L. and W.-Y.C. All authors have read and agreed to the published version of the manuscript.

Funding: This work is supported by the Natural Science Foundation of Shandong Province (No. ZR2020MA067) and the National Natural Science Foundation of China under Grant 11504202.

Data Availability Statement: Not applicable.

Acknowledgments: The calculations in this work are carried out in the Supercomputing Center of Shandong University (Weihai).

Conflicts of Interest: The authors declare no conflict of interest.

References

1. Jabeen, N.; Zaidi, A.; Hussain, A.; Hassan, N.U.; Ali, J.; Ahmed, F.; Khan, M.U.; Iqbal, N.; Elnasr, T.A.S.; Helal, M.H. Single- and Multilayered Perovskite Thin Films for Photovoltaic Applications. *Nanomaterials* **2022**, *12*, 3208. [PubMed]
2. Abir, S.S.H.; Gupta, S.K.; Ibrahim, A.; Srivastava, B.B.; Lozano, K. Tunable $CsPb(Br/Cl)_3$ perovskite nanocrystals and further advancement in designing light emitting fiber membranes. *Mater. Adv.* **2021**, *2*, 2700–2710.
3. Kirschner, M.S.; Diroll, B.T.; Guo, P.; Harvey, S.M.; Helweh, W.; Flanders, N.C.; Brumberg, A.; Watkins, N.E.; Leonard, A.A.; Evans, A.M.; et al. Photoinduced, reversible phase transitions in all-inorganic perovskite nanocrystals. *Nat. Commun.* **2019**, *10*, 504. [PubMed]
4. Moller, C.K. Crystal Structure and Photoconductivity of Caesium Plumbohalides. *Nature* **1958**, *182*, 1436. [CrossRef]
5. Ahmad, M.; Rehman, G.; Ali, L.; Shafiq, M.; Iqbal, R.; Ahmad, R.; Khan, T.; Jalali-Asadabadi, S.; Maqbool, M.; Ahmad, I. Structural, electronic and optical properties of $CsPbX_3$ (X = Cl, Br, I) for energy storage and hybrid solar cell applications. *J. Alloys Compd.* **2017**, *705*, 828–839.
6. Chen, W.; Li, X.; Li, Y.; Li, Y. A review: Crystal growth for high-performance all-inorganic perovskite solar cells. *Energy Environ. Sci.* **2020**, *13*, 1971–1996.
7. Shen, Z.; Zhao, S.; Song, D.; Xu, Z.; Qiao, B.; Song, P.; Bai, Q.; Cao, J.; Zhang, G.; Swelm, W. Improving the Quality and Luminescence Performance ofAll-Inorganic Perovskite Nanomaterials for Light-Emitting Devices by Surface Engineering. *Small* **2020**, *16*, 1907089. [CrossRef]
8. Xu, Q.; Qian, W.; Muhammad, R.; Chen, X.; Yu, X.; Song, K. Photoluminescence and Temperature Sensing Properties of Bi^{3+}/Sm^{3+} Co-Doped La_2MgSnO_6 Phosphor for Optical Thermometer. *Crystals* **2023**, *13*, 991. [CrossRef]
9. Li, B.; Yang, S.; Han, H.; Liu, H.; Zhao, H.; Li, Z.; Xu, J.; Yao, J. Highly Efficient 2D/3D Mixed-Dimensional $Cs_2PbI_2Cl_2/CsPbI_{2.5}Br_{0.5}$ Perovskite Solar Cells Prepared by Methanol/Isopropanol Treatment. *Nanomaterials* **2023**, *13*, 1239. [CrossRef]
10. Protesescu, L.; Yakunin, S.; Bodnarchuk, M.I.; Krieg, F.; Caputo, R.; Hendon, C.H.; Yang, R.X.; Walsh, A.; Kovalenko, M.V. Nanocrystals of Cesium Lead Halide Perovskites ($CsPbX_3$, X = Cl, Br, and I): Novel Optoelectronic Materials Showing Bright Emission with Wide Color Gamut. *Nano Lett.* **2015**, *15*, 3692–3696. [CrossRef]
11. Li, X.; Wu, Y.; Zhang, S.; Cai, B.; Gu, Y.; Song, J.; Zeng, H. $CsPbX_3$ Quantum Dots for Lighting and Displays: Room-Temperature Synthesis, Photoluminescence Superiorities, Underlying Origins and White Light-Emitting Diodes. *Adv. Funct. Mater.* **2016**, *26*, 2435–2445.
12. Nedelcu, G.; Protesescu, L.; Yakunin, S.; Bodnarchuk, M.I.; Grotevent, M.J.; Kovalenko, M.V. Fast Anion-Exchange in Highly Luminescent Nanocrystals of Cesium Lead Halide Perovskites ($CsPbX_3$, X = Cl, Br, I). *Nano Lett.* **2015**, *15*, 5635–5640.
13. Koscher, B.A.; Swabeck, J.K.; Bronstein, N.D.; Alivisatos, A.P. Essentially Trap-Free $CsPbBr_3$ Colloidal Nanocrystals by Postsynthetic Thiocyanate Surface Treatment. *J. Am. Chem. Soc.* **2017**, *139*, 6566–6569. [CrossRef]
14. Lu, M.; Zhang, X.; Bai, X.; Wu, H.; Shen, X.; Zhang, Y.; Zhang, W.; Zheng, W.; Song, H.; Yu, W.W.; et al. Spontaneous Silver Doping and Surface Passivation of $CsPbI_3$ Perovskite Active Layer Enable Light-Emitting Devices with an External Quantum Efficiency of 11.2%. *ACS Energy Lett.* **2018**, *3*, 1571–1577. [CrossRef]

15. Naresh, V.; Kim, B.H.; Lee, N. Synthesis of $CsPbX_3$ (X = Cl/Br, Br, and Br/I)@SiO_2/PMMA composite films as color-conversion materials for achieving tunable multi-color and white light emission. *Nano Res.* **2021**, *14*, 1187–1194. [CrossRef]
16. Liang, Z.; Zhao, S.; Xu, Z.; Qiao, B.; Song, P.; Gao, D.; Xu, X. Shape-Controlled Synthesis of All-Inorganic $CsPbBr_3$ Perovskite Nanocrystals with Bright Blue Emission. *ACS Appl. Mater. Interfaces* **2016**, *8*, 28824–28830. [CrossRef]
17. Xu, X.; He, H.; Fang, Z.; Lou, H.; Lin, C.; Chen, L.; Ye, Z. Ultrasonication-Assisted Ambient-Air Synthesis of Monodispersed Blue-Emitting $CsPbBr_3$ Quantum Dots for White Light Emission. *ACS Appl. Nano Mater.* **2019**, *2*, 6874–6879. [CrossRef]
18. Wang, H.C.; Wang, W.; Tang, A.C.; Tsai, H.Y.; Bao, Z.; Ihara, T.; Yarita, N.; Tahara, H.; Kanemitsu, Y.; Chen, S.; et al. High-Performance $CsPb_{1-x}Sn_xBr_3$ Perovskite Quantum Dots for Light-Emitting Diodes. *Angew. Chem.-Int. Ed.* **2017**, *56*, 13650–13654.
19. Li, M.; Zhang, X.; Matras-Postolek, K.; Chen, H.-S.; Yang, P. An anion-driven Sn^{2+} exchange reaction in CsPbBr3 nanocrystals towards tunable and high photoluminescence. *J. Mater. Chem. C* **2018**, *6*, 5506–5513. [CrossRef]
20. Shen, X.; Zhang, Y.; Kershaw, S.V.; Li, T.; Wang, C.; Zhang, X.; Wang, W.; Li, D.; Wang, Y.; Lu, M.; et al. Zn-Alloyed $CsPbI_3$ Nanocrystals for Highly Efficient Perovskite Light-Emitting Devices. *Nano Lett.* **2019**, *19*, 1552–1559. [CrossRef]
21. Chen, Z.; Zhou, B.; Yuan, J.; Tang, N.; Lian, L.; Qin, L.; Zhu, L.; Zhang, J.; Chen, R.; Zang, J. Cu^{2+}-Doped $CsPbI_3$ Nanocrystals with Enhanced Stability for Light-Emitting Diodes. *J. Phys. Chem. Lett.* **2021**, *12*, 3038–3045. [CrossRef] [PubMed]
22. Yu, G.; Xue, S.; Yin, R.; Wu, Q.; Gao, T.; Song, Y.; Wang, R.; Cong, W.-Y.; Guan, C.; Lu, Y.-B. How the Copper Dopant Alters the Geometric and Photoelectronic Properties of the Lead-Free $Cs_2AgSbCl_6$ Double Perovskite. *Adv. Theory Simul.* **2021**, *4*, 2100142. [CrossRef]
23. Wu, Q.; Li, J.; Xue, S.; Zhao, Y.; Liu, F.; Huo, Q.; Mi, J.; Guan, C.; Cong, W.; Lu, Y.; et al. Bandgap Engineering of Cesium Lead Halide Perovskite $CsPbBr_3$ through Cu Doping. *Adv. Theory Simul.* **2022**, *5*, 2200190. [CrossRef]
24. Bi, C.; Wang, S.; Li, Q.; Kershaw, S.V.; Tian, J.; Rogach, A.L. Thermally Stable Copper(II)-Doped Cesium Lead Halide Perovskite Quantum Dots with Strong Blue Emission. *J. Phys. Chem. Lett.* **2019**, *10*, 943–952. [CrossRef]
25. Kresse, G.; Furthmüller, J. Efficiency of ab-initio total energy calculations for metals and semiconductors using a plane-wave basis set. *Comput. Mater. Sci.* **1996**, *6*, 15–50. [CrossRef]
26. Kresse, G.; Furthmüller, J. Efficient iterative schemes for ab initio total-energy calculations using a plane-wave basis set. *Phys. Rev. B* **1996**, *54*, 11169–11186. [CrossRef]
27. Kresse, G.; Joubert, D. From ultrasoft pseudopotentials to the projector augmented-wave method. *Phys. Rev. B* **1999**, *59*, 1758–1775. [CrossRef]
28. Heyd, J.; Peralta, J.; Scuseria, G.E.; Martin, R.L. Energy band gaps and lattice parameters evaluated with the Heyd-Scuseria-Ernzerhof screened hybrid functional. *J. Chem. Phys.* **2005**, *123*, 174101. [CrossRef]
29. Blöchl, P.E.; Först, C.J.; Schimpl, J. Projector augmented wave method:ab initio molecular dynamics with full wave functions. *Bull. Mater. Sci.* **2003**, *26*, 33–41. [CrossRef]
30. Khorshidi, A.; Peterson, A.A. Amp: A modular approach to machine learning in atomistic simulations. *Comput. Phys. Commun.* **2016**, *207*, 310–324. [CrossRef]
31. Nelson, R.; Ertural, C.; George, J.; Deringer, V.L.; Hautier, G.; Dronskowski, R. LOBSTER: Local orbital projections, atomic charges, and chemical-bonding analysis fromprojector-augmented-wave-baseddensity-functional theory. *J. Comput. Chem.* **2020**, *41*, 1931–1940. [CrossRef]
32. Saidaminov, M.I.; Kim, J.; Jain, A.; Quintero-Bermudez, R.; Tan, H.; Long, G.; Tan, F.; Johnston, A.; Zhao, Y.; Voznyy, O.; et al. Suppression of atomic vacancies via incorporation of isovalent small ions to increase the stability of halide perovskite solar cells in ambient air. *Nat. Energy* **2018**, *3*, 648–654. [CrossRef]
33. Swarnkar, A.; Mir, W.J.; Nag, A. Can B-Site Doping or Alloying Improve Thermal- and Phase-Stability of All-Inorganic $CsPbX_3$ (X = CI, Br, I) Perovskites? *ACS Energy Lett.* **2018**, *3*, 286–289. [CrossRef]
34. Shannon, R.D. Revised Effective Ionic-Radii and Systematic Studies of Interatomic Distances in Halides and Chalcogenides. *Acta Crystallogr. Sect. A* **1976**, *32*, 751–767. [CrossRef]

Disclaimer/Publisher's Note: The statements, opinions and data contained in all publications are solely those of the individual author(s) and contributor(s) and not of MDPI and/or the editor(s). MDPI and/or the editor(s) disclaim responsibility for any injury to people or property resulting from any ideas, methods, instructions or products referred to in the content.